Spin diffusion in p-type bilayer WSe_2

F. Yang and M. W. Wu*

Hefei National Laboratory for Physical Sciences at the Microscale, Department of Physics, and CAS Key Laboratory of Strongly Coupled Quantum Matter Physics, University of Science and Technology of China, Hefei, Anhui 230026, China

(Received 8 April 2016; revised manuscript received 6 June 2016; published 20 June 2016)

We investigate the steady-state out-of-plane spin diffusion in p-type bilayer WSe_2 in the presence of the Rashba spin-orbit coupling and Hartree-Fock effective magnetic field. The out-of-plane components of the Rashba spin-orbit coupling serve as the opposite Zeeman-like fields in the two valleys. Together with the identical Hartree-Fock effective magnetic fields, different total effective magnetic field strengths in the two valleys are obtained. It is further revealed that due to the valley-dependent total effective magnetic field strength, similar (different) spin-diffusion lengths in the two valleys are observed at small (large) spin injection. Nevertheless, it is shown that the intervalley hole-phonon scattering can suppress the difference in the spin-diffusion lengths at large spin injection due to the spin-conserving intervalley charge transfers with the opposite transfer directions between spin-up and spin-down holes. Moreover, with a fixed large pure spin injection, we predict the buildup of a steady-state valley polarization during the spin diffusion with the maximum along the diffusion direction being capable of exceeding 1%. It is revealed that the valley polarization arises from the induced quasi-hot-hole Fermi distributions with different effective hot-hole temperatures between spin-up and spin-down holes during the spin diffusion, leading to the different intervalley charge transfer rates in the opposite transfer directions. Additionally, it is also shown that by increasing the injected spin polarization, the hole density, or the impurity density, the larger valley polarization can be obtained.

DOI: 10.1103/PhysRevB.93.235433

I. INTRODUCTION

In the past few years, monolayer (ML) and bilayer (BL) transition-metal dichalcogenides (TMDs) have attracted much attention, as they provide a promising candidate for application in spintronics due to the two-dimensionality [1–6], gate-tunable carrier concentration [7–15], and multivalley band structure [16–29]. To realize the spintronic device, a great deal of effort has been devoted to the study of the carrier spin dynamics in this material, including spin relaxation [30–38] and spin diffusion [39–41].

For spin relaxation, it has been understood that the hole spin relaxation in ML TMDs is markedly suppressed [30–32] due to the large intrinsic spin splitting [24–26]. As for the electron spin relaxation in ML TMDs, the in-plane spin-relaxation process has been revealed and it is reported that the intervalley electron-phonon scattering makes the dominant contribution [33,34]. This arises from the intrinsic spin-orbit coupling (SOC) in ML TMDs, which serves as opposite out-of-plane effective magnetic fields (EMFs) in the two valleys and hence provides the intervalley inhomogeneous broadening [42,43] for in-plane spins. For out-of-plane spins, the intrinsic D'yakonov-Perel' (DP) spin-relaxation process [44] in ML TMDs is absent due to the mirror-inversion symmetry [16–18]. Nevertheless, by breaking the mirror-inversion symmetry through the flexural phonon vibrations, the Elliot-Yafet process [45,46] can be induced to cause the electron spin relaxation [30]. In addition, with the gate-control experimental technique on carrier density [7–14], the external out-of-plane electric field leads to the Rashba SOC [47,48], and then the extrinsic DP spin relaxation of the out-of-plane electron spins has been predicted in ML TMDs [31] and confirmed by the recent experiments in ML MoS_2 [35,37].

Compared with ML TMDs, the intrinsic SOC in BL TMDs is absent due to the space-inversion symmetry. This indicates that the above-mentioned suppression of the hole spin relaxation in ML TMDs is absent in BL TMDs. In the presence of an external out-of-plane electric field E_z, the experimentally realized Rashba SOC in BL TMDs can be written as [9,10,36]

$$\mathbf{\Omega}_{\mathrm{R}}^{\mu}(\mathbf{k}) = (-\nu k_y, \nu k_x, \mu\eta) E_z, \tag{1}$$

which provides a tunable out-of-plane Zeeman-like field $\mu\eta E_z\hat{\mathbf{z}}$ with opposite directions in the two valleys. Here, ν and η are the Rashba SOC parameters; $\mu = 1\ (-1)$ represents the K (K') valley. For valley-independent out-of-plane spin polarization, the Zeeman-like field is superimposed by the identical Hartree-Fock (HF) EMF Ω_{HF} [43,52,53] in each valley, leading to the larger (smaller) total EMF $\Omega_{\mathrm{T}}^{\mu} = \mu\eta E_z + \Omega_{\mathrm{HF}}$ in the valley possessing the same (opposite) directions between $\mu\eta E_z$ and Ω_{HF}. In our previous work, we calculated the hole spin relaxation in BL WSe_2 in the presence of the Rashba SOC [36]. It is pointed out that due to the presence of the total EMF, the conventional inhomogeneous broadening in each valley is reduced by the magnetic field prefactor $(1 + |\Omega_{\mathrm{T}}^{\mu}\tau_p|^2)^{-1}$ with τ_p the momentum relaxation time, leading to the enhancement on the spin-relaxation time (SRT) [49–51]. Therefore, at small (large) spin polarization and hence weak (strong) HF EMF, identical (different) SRTs in the two valleys are obtained. Nevertheless, the intervalley hole-phonon scattering can suppress the difference in the spin polarizations and hence the SRTs between the two valleys by inducing the spin-conserving intervalley charge transfers with opposite transfer directions between spin-up and spin-down holes. Therefore, via enhancing the intervalley hole-phonon scattering, the difference in SRTs between the two

*Author to whom correspondence should be addressed: mwwu@ustc.edu.cn.

valleys at large spin polarization can be markedly suppressed. Moreover, during the spin relaxation, the quasi-hot-hole Fermi distributions with different effective hot-hole temperatures for spin-up and spin-down holes are found to be induced by the spin precessions at large spin polarization and low temperature, due to the weak hole-phonon scattering but relatively strong hole-hole Coulomb scattering. With this effective hot-hole temperature difference between spin-up and spin-down holes, the intervalley charge transfers mentioned above share different rates in the two opposite transfer directions, making the initially equal densities in the two valleys broken (refer to Fig. 1 in Ref. [36]). Hence, the valley polarization is built up.

In contrast to the spin relaxation, the study for the spin diffusion in ML and BL TMDs is so far rarely reported in the literature. In ML TMDs, it has been reported that the intravalley scattering makes the dominant contribution during the in-plane spin diffusion whereas the intervalley one is marginal [39]. This is different from the in-plane spin relaxation [32], where the intervalley scattering plays an important role. For BL TMDs, in the presence of the Rashba SOC and HF EMF, rich physics of the out-of-plane spin diffusion can be expected. Specifically, the spin spatial precession frequency in each valley is determined by [54–56]

$$\boldsymbol{\omega}_{\mathbf{k}}^{\mu} = \frac{m}{k_x}\left(\boldsymbol{\Omega}_{\mathrm{R}}^{\mu} + \boldsymbol{\Omega}_{\mathrm{HF}}\right) = m\left(-\nu E_z \frac{k_y}{k_x}, \nu E_z, \frac{\Omega_{\mathrm{T}}^{\mu}}{k_x}\right) \quad (2)$$

when the diffusion is along the $\hat{\mathbf{x}}$ direction. Here, m stands for the effective mass of holes. It is noted that the previous work on ultracold ^{40}K gas by Yu and Wu [57] shares similar spin spatial precession frequency [$\boldsymbol{\omega}(\mathbf{k}) = m(\Omega/k_x, 0, \alpha)$ with Ω acting as an EMF, α being the SOC strength, and the spin polarization parallel to EMF], except for an additional field $(m\nu E_z k_y/k_x, 0, 0)$ perpendicular to EMF in BL WSe_2 which provides the inhomogeneous broadening [42,43,54–56]. Accordingly, in comparison with the rich regimes of the spin diffusion in cold atoms [57], different and rich spin-diffusion features in each valley are anticipated in BL WSe_2. Moreover, due to the valley-dependent total EMF strength, different spin-diffusion lengths in the two valleys can be obtained at the weak intervalley scattering. Furthermore, in the presence of the spin spatial precessions, the quasi-hot-hole Fermi distributions with different effective hot-hole temperatures between spin-up and spin-down holes are expected at large spin injection and low temperature. Hence, similarly to the induced valley polarization in the time domain as mentioned above [36], one may also expect a steady-state valley polarization in the spatial domain.

In the present work, by the kinetic spin Bloch equation (KSBE) approach [43], we investigate the steady-state out-of-plane spin diffusion in p-type BL WSe_2 with all the relevant scatterings included. Both cases with and without the intervalley scattering (intervalley hole-phonon scattering) are studied. For the case without the intervalley scattering, the spin-diffusion processes in the two valleys are independent, and it shown that the spin-diffusion system in each valley can be divided into four regimes by tuning the total EMF strength in the corresponding valley, similarly to the rich regimes of the spin diffusion in cold atoms mentioned above [57]. In each regime, the spin-diffusion length shows different dependencies on the scattering, total EMF, and SOC strengths. At small (large) injected spin polarization and hence the weak (strong) HF EMF, the total EMFs, determined by the Zeeman-like fields (Zeeman-like fields and HF EMFs), possess identical (different) strengths in the two valleys. Therefore, similar (different) spin-diffusion lengths in the two valleys are observed.

When the intervalley hole-phonon scattering is included, the difference in the spin-diffusion lengths in the two valleys is suppressed. Specifically, at large spin injection, with the different spin-diffusion lengths and hence the different spin polarizations along the diffusion direction in the two valleys, the spin-conserving intervalley charge transfers with opposite transfer directions between spin-up and spin-down holes are triggered, which tends to suppress the difference in the spin polarizations. The suppression is found to become stronger with the enhancement of the intervalley hole-phonon scattering. Moreover, with a fixed single-side large pure spin injection, we find that a steady-state valley polarization along the spin-diffusion direction is built up at low temperature. It is further revealed that the valley polarization is induced by the different intervalley charge transfer rates between spin-up and spin-down holes, which possess opposite transfer directions. The difference in the intervalley charge transfer rates here arises from the induced quasi-hot-hole Fermi distributions with different effective hot-hole temperatures between the spin-up and spin-down holes during the spin diffusion. In addition, it is found that by increasing the impurity density, the maximum valley polarization along the diffusion direction can be markedly enhanced. This is very different from the time domain, in which the maximum valley polarization is always suppressed with the increase of the intravalley scattering strength. With the physics of this unique enhancement further revealed, it is shown that larger valley polarization can be reached by increasing the hole density and/or injected spin polarization at large impurity density. Particularly, at the experimental obtainable hole density and injected spin polarization, we report that the maximum valley polarization along the diffusion direction can exceed 1%, providing the possibility for the experimental detection.

This paper is organized as follows. In Sec. II, we introduce our model and lay out the KSBEs. Then in Sec. III, we study the out-of-plane spin diffusion both analytically and numerically without the intervalley hole-phonon scattering. In Sec. IV, we show the influence of the intervalley hole-phonon scattering on the out-of-plane spin diffusion. The investigation of the induced valley polarization during the spin diffusion is also addressed in this part. We summarize in Sec. V.

II. MODEL AND KSBEs

In the presence of an out-of-plane electric field, the effective Hamiltonian of the lowest two hole bands near the K (K') point in BL WSe_2 is given by [9]

$$H_{\mathrm{eff}}^{\mu} = \varepsilon_{\mathbf{k}} + \boldsymbol{\Omega}_R^{\mu} \cdot \mathbf{s}, \quad (3)$$

where $\varepsilon_{\mathbf{k}} = \mathbf{k}^2/(2m)$; $\mathbf{s}$ denotes the spin vector and the Rashba SOC $\boldsymbol{\Omega}_{\mathrm{R}}^{\mu}$ is given in Eq. (1).

The microscopic KSBEs, constructed to investigate the hole spin diffusion in BL TMDs, can be written as [43]

$$\dot{\rho}_{\mu\mathbf{k}}(\mathbf{r},t) = \dot{\rho}_{\mu\mathbf{k}}(\mathbf{r},t)|_{\rm coh} + \dot{\rho}_{\mu\mathbf{k}}(\mathbf{r},t)|_{\rm diff} + \dot{\rho}_{\mu\mathbf{k}}(\mathbf{r},t)|_{\rm scat}, \quad (4)$$

where $\dot{\rho}_{\mu\mathbf{k}}(\mathbf{r},t)$ represent the time derivatives of the density matrices of hole with momentum $\mathbf{k}$ at position $\mathbf{r} = (x,y)$ and time t, in which the off-diagonal elements $\rho_{\mu\mathbf{k},\sigma-\sigma}$ describe the spin coherence and the diagonal ones $\rho_{\mu\mathbf{k},\sigma\sigma}$ represent the hole distribution functions.

The coherent terms [58], describing the spin precessions of holes due to the Rashba SOC $\mathbf{\Omega}_R^\mu$ and the HF EMF $\mathbf{\Omega}_{\rm HF}$, are given by

$$\dot{\rho}_{\mu\mathbf{k}}(\mathbf{r},t)|_{\rm coh} = -i\left[\mathbf{\Omega}_{\rm R}^\mu \cdot \mathbf{s} + \mathbf{\Omega}_{\rm HF} \cdot \mathbf{s}, \rho_{\mu\mathbf{k}}\right], \quad (5)$$

where [,] denotes the commutator. The HF EMF, from the Coulomb HF self-energy [43,51–53], reads

$$\mathbf{\Omega}_{\rm HF}(\mathbf{k}) = -\sum_{\mathbf{k}'} V_{\mathbf{k}-\mathbf{k}'} {\rm Tr}[\rho_{\mu\mathbf{k}'}\boldsymbol{\sigma}], \quad (6)$$

with $V_{\mathbf{k}-\mathbf{k}'}$ being the screened Coulomb potential. It is noted that for valley-independent spin injection, the HF EMFs are identical in the two valleys. The diffusion terms for the spin diffusion along the $\hat{\mathbf{x}}$ direction are written as

$$\dot{\rho}_{\mu\mathbf{k}}(\mathbf{r},t)|_{\rm diff} = -(k_x/m)\partial_x \rho_{\mu\mathbf{k}}(\mathbf{r},t). \quad (7)$$

For the scattering terms $\dot{\rho}_{\mu\mathbf{k}}(\mathbf{r},t)|_{\rm scat}$, we include all the relevant scatterings, i.e., the hole-hole Coulomb, long-range hole-impurity, intravalley hole-in-plane-acoustic-phonon, hole-in-plane- and hole-out-of-plane-optical-phonon, and intervalley hole-$K_6^{\rm L}$- and hole-$K_6^{\rm H}$-phonon scatterings. All these scatterings are the spin-conserving ones. Here, $K_6^{\rm L}$ ($K_6^{\rm H}$) is the phonon mode at the K point corresponding to the irreducible representation E_2'' of group C_{3h} with the lower (higher) phonon energy [30]. The detailed expressions of the above scatterings and the corresponding scattering matrix elements are given in our previous work [36].

In the numerical calculation, the KSBEs are solved by taking the fixed double-side boundary conditions [54]

$$\rho_{\mu\mathbf{k}}(x=0,t) = \frac{f_{\mu\mathbf{k}\uparrow}+f_{\mu\mathbf{k}\downarrow}}{2} + \frac{f_{\mu\mathbf{k}\uparrow}-f_{\mu\mathbf{k}\downarrow}}{2}\sigma_z, \quad k_x > 0,$$
$$\rho_{\mu\mathbf{k}}(x=L,t) = f^0_{\mu\mathbf{k}}, \quad k_x < 0, \quad (8)$$

with the spin injection from the left side. Here, $f_{\mu\mathbf{k}\sigma} = \{\exp[(\epsilon_{\mathbf{k}} - \mu_{\mu\sigma})/(k_B T)] + 1\}^{-1}$ with $\mu_{\mu\sigma}$ being the chemical potential determined by the hole density and the injected spin polarization P_s^0; $f^0_{\mu\mathbf{k}}$ is the Fermi distribution at equilibrium. For these boundary conditions, the states with $k_x > 0$ at the left edge $x = 0$ are assumed to be the source of the spin injection. The sample length L is chosen to be large enough (far larger than the spin-diffusion length) so that the spin polarization vanished before it reaches the right edge. States with $k_x < 0$ ($k_x > 0$) in the interior ($0 < x < L$) are determined from the right (left) side of the sample with zero (fixed injected) spin polarization. The hole densities are equal in the two valleys at $x = 0$, and hence no valley-polarization injection occurs. Moreover, with the same hole density and hence same chemical potential in the system, no charge diffusion occurs. All the material parameters used in our calculation are given in Ref. [36]. The Fermi energy in the calculation is chosen to be larger than the effective Rashba SOC energy.

III. INTRAVALLEY PROCESS

It is noted that in each valley, the spin spatial precession frequency [Eq. (2)] is very similar to that in the previous work on ultracold ^{40}K gas by Yu and Wu [57] except for an additional field $mvE_z(k_y/k_x,0,0)$ in BL WSe_2. Accordingly, similarly to the rich regimes of the spin diffusion in cold atoms, rich intravalley spin-diffusion features are anticipated in BL WSe_2. In our calculation, it is found that the intervalley hole-phonon scattering is marginal at small spin injection and becomes important only at large spin injection. This indicates that the spin-diffusion is determined by the intravalley process at small spin injection. Therefore, in this section, we first investigate the steady-state out-of-plane spin diffusion at small spin injection without the intervalley hole-phonon scattering. The case at large spin injection without the intervalley hole-phonon scattering is also addressed in this section to facilitate the understanding of the complete picture in the next section. Features of the spin diffusions in the two valleys in this section are independent and determined solely by the intravalley spin-diffusion processes.

A. Analytical results

We first focus on the analytical study by simplifying the KSBEs [Eq. (4)] with only the hole-impurity scattering in the scattering terms. In the steady state, the Fourier components of the density matrix with respect to θ_k are given by

$$\begin{aligned} &kvE_z\left(\left[s_-,\rho_{\mu k}^{l-1}\right] - \left[s_+,\rho_{\mu k}^{l+1}\right]\right)/2 - i\Omega_{\rm T}^\mu\left[s_z,\rho_{\mu k}^l\right] \\ &\quad = k/(2m)\partial_x\left(\rho_{\mu k}^{l-1} + \rho_{\mu k}^{l+1}\right) + \rho_{\mu k}^l/\tau_{k,l}, \end{aligned} \quad (9)$$

with $\tau_{k,l}^{-1} = \frac{N_i m}{2\pi}\int_0^{2\pi} d\theta_{\mathbf{k}} |V_{\mathbf{k}-\mathbf{k}'}|^2(1-\cos l\theta_{\mathbf{k}})$ and $N_{\rm i}$ being impurity density.

In the strong ($l_\tau \ll l_v, l_{\Omega_{\rm T}^\mu}$) and moderate ($l_{\Omega_{\rm T}^\mu} \ll l_\tau \ll l_v$) scattering regimes, one only needs to keep the lowest two orders ($l = 0,1$) [59], and obtains the analytical solution for the spin polarization along the diffusion direction from Eq. (9) (refer to Appendix A). Following the previous work on ultracold ^{40}K gas [57], by incorporating the additional field $(mvE_z k_y/k_x,0,0)$ in BL WSe_2, we define three characteristic lengths: the mean-free path $l_\tau = k\tau_p/m$, the SOC length $l_v = 1/|vE_M|$, and the total EMF length $l_{\Omega_{\rm T}^\mu} = k/|\Omega_{\rm T}^\mu m|$ in each valley, and show that the spin-diffusion system can be divided into four regimes: I, the large total EMF and moderate scattering regime ($l_\tau \ll l_{\Omega_{\rm T}^\mu} \ll l_v$); II, the large total EMF and strong scattering regime ($l_{\Omega_{\rm T}^\mu} \ll l_\tau \ll l_v$); III, the crossover regime ($l_\tau \ll l_v \ll l_{\Omega_{\rm T}^\mu} \ll 2l_v^2/l_\tau$); IV, the small total EMF regime ($l_\tau \ll l_v \ll 2l_v^2/l_\tau \ll l_{\Omega_{\rm T}^\mu}$). In different regimes, the spin polarizations exhibit different decay behaviors and the corresponding decay lengths show different dependencies on the scattering, SOC, and total EMF strengths. The specific spin-polarization behaviors in each regime are summarized in Table I.

TABLE I. Behaviors of the steady-state out-of-plane spin polarization along the diffusion direction and the corresponding spin-diffusion lengths in each regime. $l_c = 2l_v^2/l_\tau$.

Regime	Condition	Behavior	Decay length l_s
I: Large total EMF and moderate scattering regime	$l_{\Omega_T^\mu} \ll l_\tau \ll l_v$	single-exponential decay	$l_\tau l_v/(\sqrt{6}l_{\Omega_T^\mu})$
II: Large total EMF and strong scattering regime	$l_\tau \ll l_{\Omega_T^\mu} \ll l_v$	single-exponential decay	$l_v\left(1+l_\tau^2/l_{\Omega_T^\mu}^2\right)/\sqrt{2}$
III: Crossover regime	$l_\tau \ll l_v \ll l_{\Omega_T^\mu} \ll l_c$	single-exponential decay	$l_v\left(1-2l_{\Omega_T^\mu}^2/l_c^2\right)/\sqrt{2}$
		oscillatory decay	$\sqrt{l_\tau l_{\Omega_T^\mu}}$
IV: Small total EMF regime	$l_\tau \ll l_v \ll l_c \ll l_{\Omega_T^\mu}$	oscillatory decay	$l_v/(2\sqrt{2\sqrt{2}-1})$

It is noted that from Eq. (2), the direction of the inhomogeneous broadening $\hat{\mathbf{z}}'$, given by

$$\hat{\mathbf{z}}' = \frac{1}{\sqrt{1+\left|\Omega_T^\mu/(vkE_z)\right|^2}}\hat{\boldsymbol{\theta}}_{\boldsymbol{k}} + \frac{\Omega_T^\mu/(vkE_z)}{\sqrt{1+\left|\Omega_T^\mu/(vkE_z)\right|^2}}\hat{\mathbf{z}}, \quad (10)$$

is nearly along the $\hat{\mathbf{z}}$ direction in the large total EMF regimes (regimes I and II with $|\Omega_T^\mu|/|vkE_z| \gg 1$). Therefore, the out-of-plane spins cannot precess around the inhomogeneous broadening effectively. In this situation, the spin polarization decays without any oscillation, and through the modified drift-diffusion model [$l_s = \sqrt{D\tau_s}$ with the diffusion coefficient [60,61] $D = v_F^2\tau_p/3$ (v_F represents the Fermi velocity) and SRT $\tau_s = (1+|\Omega_T^\mu\tau_p|^2)/(|vkE_z|^2\tau_p)$] proposed by Yu and Wu in cold atoms [57], the spin diffusion in our work can be understood well.

As for the crossover regime (regime III) and the small total EMF regime (regime IV), with $|\Omega_T^\mu|/|vkE_z| \ll 1$, the direction of the inhomogeneous broadening $\hat{\mathbf{z}}'$ [Eq. (10)] deviates from that of the out-of-plane spin polarization, and hence the efficient spin precessions are induced. It has been pointed out by Yu and Wu [57] that the modified drift-diffusion model fails to explain the spin diffusion in this situation. In the present work, we suggest a reasonable picture based on the previous works in semiconductor [62] and graphene [63] to facilitate the understanding of the spin diffusion in regimes III and IV. Specifically, as seen from Eq. (2), there are two channels for the out-of-plane spin diffusion: (i) through the inhomogeneous broadening provided by the conventional Rashba SOC, i.e., the additional field $mvE_z(k_y/k_x,0,0)$ [63]; (ii) by rotating out-of-plane spins into the in-plane direction via spin spatial precessions and then through the inhomogeneous broadening for in-plane spins provided by the total EMF [62]. In the crossover regime (regime III), both channel (i) and (ii) are important. Nevertheless, the presence of the total EMF suppresses the out-of-plane spin precessions induced by the conventional Rashba SOC, and the suppression should decrease with the increase of $|vE_zk/\Omega_T^\mu|^2 = l_{\Omega_T^\mu}^2/l_v^2$ according to Eq. (10). Therefore, the spin polarization through channel (i) shows single-exponential decay with the decay length $l_s^s \approx l_v(1-2l_{\Omega_T^\mu}^2 l_\tau^2/l_v^4)/\sqrt{2}$. In addition, the spin polarization through channel (ii) shows the oscillatory decay with the decay length $l_s^o \approx \sqrt{l_\tau l_{\Omega_T^\mu}}$ [62]. Consequently, the spin polarization in regime III is approximated by one oscillatory decay together with one single-exponential decay. With further decreasing the total EMF, the system enters the small total EMF regime (regime IV). In this regime, due to the weak total EMF, the inhomogeneous broadening in channel (ii) becomes inefficient, while the suppression from the total EMF on channel (i) also becomes weak. Consequently, the spin polarization, only determined by channel (i) without any suppression, shows the oscillatory decay with the decay length $l_s = l_v/(2\sqrt{2\sqrt{2}-1})$, the same as the work in graphene [63].

B. Numerical results

We next discuss the spin diffusion without the intervalley scatterings by numerically solving the KSBEs at small and large spin injections. To compare with the analytical results revealed in Sec. III A, both cases with only the long-range hole-impurity scattering and with all the intravalley scatterings are studied.

1. *Scattering strength dependence*

In this part, we address the scattering strength dependence of the intravalley spin-diffusion process. We first focus on the case with only the long-range hole-impurity scattering. The spin-diffusion lengths as a function of impurity density at different hole densities are plotted in Figs. 1(a) and 1(b) with small ($P_s^0 = 2.5\%$) and large ($P_s^0 = 30\%$) injected spin polarizations, respectively. At small injected spin polarization and hence the weak HF EMF, the total EMFs, determined by the large Zeeman-like fields, have identical strengths in the two valleys. Consequently, from Table I, the systems in the K and K' valleys both sit in the large total EMF regimes and same spin-diffusion lengths in the two valleys are obtained. When $N_i/N_h < 0.2$, the system lies in the moderate scattering regime (regime I), and the spin-diffusion length $l_s \propto \tau_p|\Omega_T^\mu|$. It is noted that the hole-impurity scattering strength $1/\tau_p^i \propto N_i/N_h$ [64]. Therefore, the increase of N_i/N_h leads to the decrease of the spin-diffusion length when $N_i/N_h < 0.2$, as shown in Fig. 1(a). By further increasing the scattering strength to the strong scattering regime (regime II), the spin-diffusion length $l_s \approx l_v/\sqrt{2}$ becomes scattering-independent when $N_i/N_h > 0.2$. Moreover, some marginal difference in the spin-diffusion lengths between the two valleys is observed in the moderate scattering regime. This is due to the weak HF EMFs at small spin injection, which lead to the small difference in the total EMFs. Additionally, identical spin diffusion lengths in the two valleys are obtained from the analytical results [obtained from Eq. (A6) by setting $\Omega_T^\mu = \mu\eta E_z$], as shown by the dot-dashed curve in Fig. 1(a). It is found that the analytical results agree with the numerical ones (solid curves) fairly well in the strong

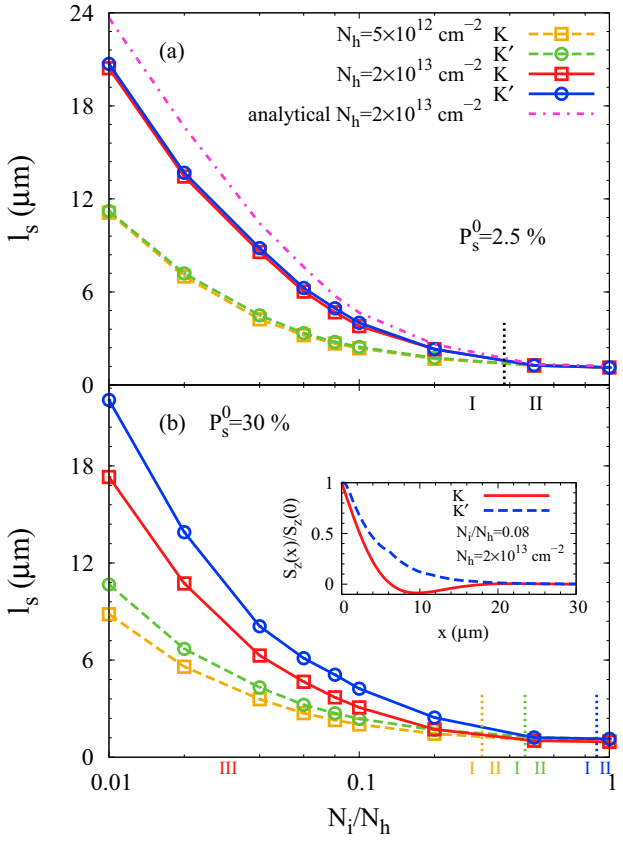

FIG. 1. Scattering dependence of the spin-diffusion length with only the long-range hole-impurity scattering at different hole densities when (a) $P_s^0 = 2.5\%$ and (b) $P_s^0 = 30\%$. Squares (Circles): in the K (K') valley. The dot-dashed curve in the figure is calculated from the analytical result [obtained from Eq. (A6) by setting $\Omega_T^\mu = \mu\eta E_z$]. The dotted lines on the panels indicate the boundaries between regimes I and II. Particularly, the boundaries between regimes I and II in (a) for different curves are located at the same position. The roman numbers with the color at the bottom panel indicate the regimes of the corresponding systems denoted by the same color. The inset in (b) shows the spin polarizations along the diffusion direction in the K (solid curve) and K' (dashed curve) valleys. $E_z = 0.02$ V/Å.

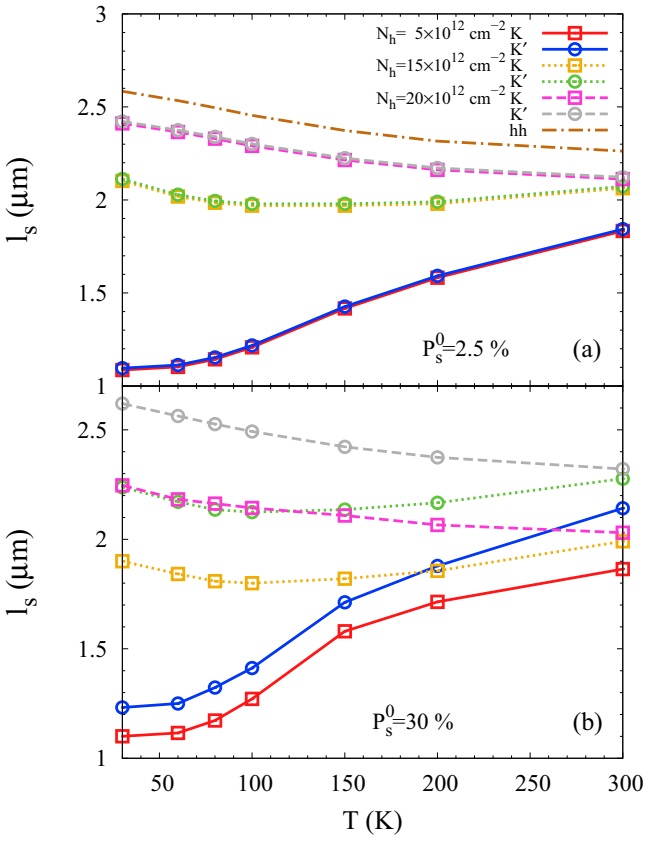

FIG. 2. The spin-diffusion length versus temperature T at different hole densities when (a) $P_s^0 = 2.5\%$ and (b) $P_s^0 = 30\%$. Squares (Circles): in the K (K') valley with all the intravalley scatterings included. Dot-dashed curve: with only the hole-hole Coulomb scattering included at $N_h = 2 \times 10^{13}$ cm^{-2}. $E_z = 0.02$ V/Å.

scattering regime and are very close to the numerical ones in the moderate scattering regime.

At large injected spin polarization and hence the strong HF EMF, the total EMFs have different strengths in the two valleys, leading to different spin-diffusion lengths according to Table I. Specifically, in our calculation, the HF EMF and Zeeman-like field have the opposite (same) directions in the K (K') valley, and hence the total EMF has a larger strength in the K' valley. At $N_h = 5 \times 10^{12}$ cm^{-2} (dashed curves), the HF EMFs ($\Omega_{HF} \approx 1.86$ meV) are relatively smaller than the Zeeman-like fields ($\eta E_z = 10.6$ meV), and hence systems in the K and K' valleys sit in the large total EMF regimes (regimes I and II). Consequently, when $N_i/N_h < 0.2$ (regime I with $l_s \propto \tau_p|\Omega_T^\mu|$), the spin-diffusion length in the K' valley (curves with circles) is larger than that in the K one (curves with squares), as shown in Fig. 1(b). At $N_h = 2 \times 10^{13}$ cm^{-2}, the HF EMF ($\Omega_{HF} = 7.95$ meV) is relatively strong. In this situation, the system in the K (K') valley lies in the crossover regime (large total EMF regimes). As shown in the inset of Fig. 1(b), the spin polarization in the K (K') valley [solid curves (dot-dashed curves)] shows the oscillatory (single-exponential) decay along the diffusion direction, consistent with the analytical results. Moreover, according to Table I, it is found that the spin-diffusion length in the K' valley is also larger than that in the K one, and the spin-diffusion length in the K (K') valley decreases with the increase of the scattering strength.

We next take all the relevant intravalley scatterings (hole-hole Coulomb, long-range hole-impurity, and intravalley hole-phonon scatterings) into account. The impurity density is taken to be $N_i = 0.02N_h$ according to Ref. [36]. The spin-diffusion lengths as a function of temperature at different hole densities are plotted in Figs. 2(a) and 2(b) with small ($P_s^0 = 2.5\%$) and large ($P_s^0 = 30\%$) injected spin polarizations, respectively. As seen from the figure, different (nearly identical) spin-diffusion lengths in the two valleys are obtained at large (small) injected spin polarization. In addition, it is found that in each valley, with the increase of the temperature, the spin-diffusion lengths at small and large spin polarizations both increase at low hole density $N_h = 5 \times 10^{12}$ cm^{-2} (solid curves) but decrease at high hole density $N_h = 2 \times 10^{13}$ cm^{-2} (dashed curves). This is due to the dominant hole-hole Coulomb scattering in BL WSe_2. Specifically, as shown in Fig. 2(a), the spin-diffusion length at $N_h = 2 \times 10^{13}$ cm^{-2} with all the intravalley

scattering (dashed curves) is close to that with only the hole-hole Coulomb scattering (dot-dashed curve). This indicates that the hole-hole Coulomb scattering makes dominant contribution in the spin diffusion. Moreover, from the results with only the hole-impurity scattering (Fig. 1), it has been demonstrated that in each valley, with the decrease of τ_p, the spin-diffusion lengths at small and large spin injection both decrease monotonically before the scattering becomes very strong, and then saturate around $l_s \approx l_v/\sqrt{2}$ ($l_v/\sqrt{2} \approx 0.82\,\mu$m). When all the intravalley scatterings are included, as shown in Figs. 2(a) and 2(b), the spin-diffusion length in each valley is larger than $l_v/\sqrt{2}$. Consequently, with the dominant hole-hole Coulomb scattering strength $1/\tau_p^{\rm hh} \propto \ln(T_F/T)T^2/T_F$ ($1/\tau_p^{\rm hh} \propto 1/T$) at $T \ll (\gg) T_F$ [65,66], the spin-diffusion length decreases (increases) with the increase of temperature in the degenerate (nondegenerate) limit for high (low) hole density. Therefore, as shown in Figs. 2(a) and 2(b), at hole density $N_h = 1.5 \times 10^{13}$ cm^{-2} (dotted curves) with $T_F \approx 410$ K, a valley shows up at the crossover from the degenerate to nondegenerate limits ($T_c \approx T_F/4$ in p-type BL WSe_2 [36]) in the temperature dependence of the spin-diffusion length.

2. Total EMF dependence

Next we turn to study the total EMF dependence of the spin-diffusion length with all the intravalley scatterings included. The spin-diffusion lengths as a function of the injected spin polarization without the intervalley scattering are plotted by dashed curves in Figs. 3(a) and 3(b) at low ($T = 30$ K) and high ($T = 300$ K) temperatures, respectively. At small injected spin polarization ($P_s^0 < 30\%$), total EMF is determined by the Zeeman-like field, and systems in the K and K' valley both sit in the large total EMF and moderate scattering regime (regime I with $l_s \propto |\Omega_{\rm T}^{\mu}|$). It has been mentioned above that the HF EMF and Zeeman-like field possess opposite (the same) directions in the K (K') valley in our calculation. Consequently, with the increase of the injected spin polarization and hence the HF EMF strength, the total EMF strength in the K (K') valley becomes weaker (stronger), leading to the decrease (increase) of the spin-diffusion length [dashed curve with squares (circles)] when $P_s^0 < 30\%$, as shown in Figs. 3(a) and 3(b).

Moreover, by further increasing the injected spin polarization, the system in the K valley enters the crossover regime (regime III) when $P_s^0 > 30\%$ and that in the K' one still sits in regime I, as mentioned above. Consequently, the spin-diffusion length in the K' valley (dashed curve with circles) still increases rapidly with the injected spin polarization. However, it is noted that with the increase of the injected spin polarization, i.e., the decrease of the total EMF strength in the K valley, the spin-diffusion length in this valley (dashed curve with squares) decreases. This is hard to understand directly from Table I, where it is shown that both single-exponential decay and oscillatory decay of the spin polarization can happen in regime III. As mentioned above, the decrease of the total EMF enhances the single-exponential-decay channel [channel (i)] and suppresses the oscillatory-decay channel [channel (ii)]. From our calculation, with all the intravalley scatterings, it is found that channel (i) is more important when $P_s^0 > 30\%$, leading to the decrease of the spin-diffusion length in the K valley with decreasing the total EMF strength.

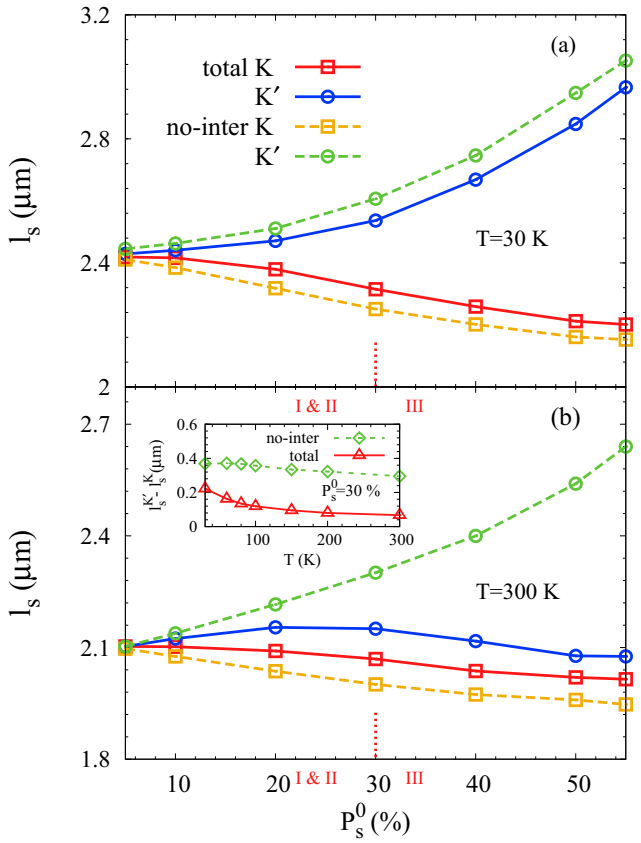

FIG. 3. The spin-diffusion length as function of injected spin polarization P_s^0 when (a) $T = 30$ K and (b) $T = 300$ K. Squares (Circles): in the K (K') valley. Solid (Dashed) curves: with (without) the intervalley hole-phonon scattering. The dotted lines on the panels indicate the boundaries between the large total EMF regimes (regimes I and II) and the crossover regime (regime III) in the K' valley, and the roman numbers at the bottom of the panels indicate the corresponding regimes. It is noted that for the large total EMF regimes (regimes I and II) in the K' valley (when $P_s^0 < 30\%$), the boundary between regimes I and II ($|\Omega_{\rm T}^{K'}\tau_p| \approx 1$) is hard to determine due to the above-mentioned dominant hole-hole Coulomb scattering in τ_p. The system in the K valley always sits in regime I. The inset in (b) shows the difference in the spin-diffusion lengths $l_s^{K'} - l_s^K$ between the two valleys versus temperature T. Triangles (Diamonds): with (without) the intervalley hole-phonon scattering. $N_h = 2 \times 10^{13}$ cm^{-2} and $E_z = 0.02$ V/Å.

IV. ROLE OF THE INTERVALLEY SCATTERING

As mentioned above, it is found that the intervalley hole-phonon scattering is marginal at small spin injection and becomes important only at large spin injection. Therefore, we next investigate the role of the intervalley hole-phonon scattering on the out-of-plane spin diffusion at large spin injection. Two aspects of the influence are studied.

On one hand, at large spin injection, with the smaller spin-diffusion length in the K valley in our calculation, the faster decay of the spin polarization along the diffusion direction makes the density of spin-down (spin-up) holes larger (smaller) in this valley than in the K' one, triggering the spin-conserving intervalley charge transfer of spin-down (spin-up) holes from the K (K') valley to the K' (K) one through the intervalley hole-phonon scattering. Consequently,

the difference in the spin polarizations and hence the difference in the spin-diffusion lengths between the two valleys is suppressed.

On the other hand, it has been pointed out in the previous works [33,34] that for the in-plane spin relaxation (in the time domain) in ML MoS_2, the valley-dependent EMF provides the intervalley inhomogeneous broadening for in-plane spins, and opens an intervalley in-plane spin-relaxation channel in the presence of the intervalley scattering. Similarly to the time domain, the total EMF in the spatial domain [Eq. (2)] is also valley-dependent in BL WSe_2, leading to the intervalley in-plane spin-decay channel during the spin diffusion when the intervalley scattering is included. For the out-of-plane spin diffusion, the system in the K valley at large spin injection (with small total EMF) sits in the crossover regime, and hence the out-of-plane spins in this valley can precess efficiently into the in-plane direction, activating the intervalley spin-decay channel revealed above.

Finally, in the presence of the intervalley hole-phonon scattering, it is interesting to find that a steady-state valley polarization is built up during the spin diffusion at large spin injection and low temperature. We systematically investigate this interplay of the spin polarization with the valley polarization in the spatial domain, and find that the valley polarization arises from the quasi-hot-hole Fermi distributions with different effective hot-hole temperatures between spin-up and spin-down holes, which are induced during the spin diffusion, similarly to the induced valley polarization during the spin relaxation (in the time domain) [36].

A. Spin diffusion

In this part, we analyze the out-of-plane spin diffusion with both the intra- and intervalley scatterings. The spin-diffusion lengths as a function of the injected spin polarization with all the relevant scatterings included are plotted by solid curves in Figs. 3(a) and 3(b) at low ($T = 30$ K) and high ($T = 300$ K) temperatures, respectively. With the intervalley hole-phonon scattering, the spin-conserving intervalley charge transfer is switched on, leading to the difference in the spin-diffusion lengths in the two valleys suppressed, as mentioned above. At low (high) temperature $T = 30$ K ($T = 300$ K), as seen from Fig. 3(a) [Fig. 3(b)], the suppression is weak (strong) due to the weak (strong) intervalley hole-phonon scattering, and hence different (similar) spin-diffusion lengths can be obtained. The differences in the spin-diffusion lengths between the two valleys versus temperature are plotted in the inset of Fig. 3(b) with (solid curve with triangles) and without (dashed curve with diamonds) the intervalley hole-phonon scattering. As seen from the inset, the suppression on the difference in the spin-diffusion lengths in the two valleys becomes stronger with the enhancement of the intervalley hole-phonon scattering by increasing temperature.

In Fig. 4, we further plot the spin-diffusion length versus temperature at large spin injection with all the relevant scatterings included. Comparing the results with (Fig. 4) and without [Fig. 2(b)] the intervalley hole-phonon scattering, we find that the leading role of the intervalley hole-phonon scattering on the out-of-plane spin diffusion is to suppress the difference in the spin-diffusion lengths between the two

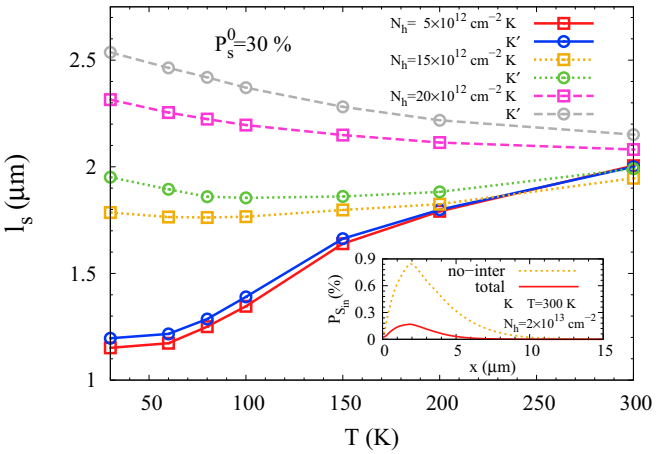

FIG. 4. The temperature dependence of the spin-diffusion length with all the relevant scatterings included at different hole densities when $P_s^0 = 30\%$. Squares (Circles): in the K (K') valley. The inset shows the induced in-plane spin polarization in the K valley during the out-of-plane spin diffusion with (solid curve) and without (dotted curve) the intervalley hole-phonon scattering. $E_z = 0.02$ V/Å.

valleys. Moreover, our study shows that the intervalley spin-decay channel mentioned above is always inefficient during the out-of-plane spin diffusion. This is because the intervalley charge transfer tends to suppress the difference in the spin polarizations in the two valleys. With this suppression, the efficient spin precessions in the K valley due to the small total EMF can be effectively suppressed by the large total EMF in the K' valley. The in-plane spin polarization in the K valley during the out-of-plane spin diffusion, which is induced by the spin spatial precessions, is plotted in the inset of Fig. 4(b). As seen from the inset, in contrast to the result without the intervalley hole-phonon scattering (dotted curve), the induced in-plane spin polarization in the K valley is markedly suppressed when the intervalley hole-phonon scattering is switched on (solid curve), leading to the intervalley spin-decay channel inefficiency.

B. Valley polarization

As mentioned in the introduction, with the different spin-diffusion lengths in the two valleys at large spin injection, a steady-state valley polarization is expected to build up during the spin diffusion at low temperature, similarly to the valley polarization in the time domain [36]. Specifically, it has been mentioned above that the intervalley charge transfers possess opposite transfer directions between the spin-up (from the K' valley to the K one) and spin-down holes (from the K valley to the K' one). Moreover, as shown in Fig. 6 where the steady-state distributions for spin-up and spin-down holes in the K valley at $x = 1$ μm are plotted, we find that the hole distributions during the spin diffusion exhibit the quasi-hot-hole Fermi distribution behaviors, and the effective hot-hole temperature of the $k_x > 0$ ($k_x < 0$) states in the distribution [72 K (62 K)] for spin-down holes [solid (dashed) curve] is larger than that [68 K (59 K)] for spin-up ones [dot-dashed (dotted) curve], leading to the intervalley charge transfer of spin-down holes faster than that

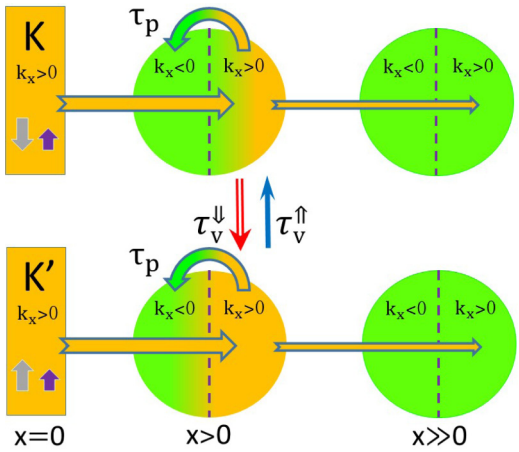

FIG. 5. Schematic of the spin-diffusion processes in the two valleys and valley polarization process. In the figure, the purple (gray) filled arrows, which have the same (opposite) directions in the two valleys, stand for the HF (Zeeman-like) EMFs; the brown (green) color denotes the states with $P_s \neq 0$ ($P_s = 0$). On one hand, this schematic shows that due to the smaller total EMF and hence the smaller spin-diffusion length in the K valley, the spin polarization in this valley is smaller than that in the K' one, inducing the intervalley charge transfers with opposite transfer directions between the spin-up [from the K' valley to the K one (blue single arrow)] and spin-down holes [from the K valley to the K' one (red double arrow)]. The intervalley charge transfer rate $1/\tau_v^{\Downarrow}$ for spin-down holes is faster than that $1/\tau_v^{\Uparrow}$ for spin-up ones due to the larger effective hot-hole temperature for spin-down holes (refer to Fig. 1 in Ref. [36]). On the other hand, this schematic exhibits that in the region away from the boundary ($x > 0$), $P^{\mu}_{s,k_x>0}$ is induced due to the spin injection from the boundary ($x = 0$) through the $k_x > 0$ states and $P^{\mu}_{s,k_x<0}$ is induced through the scattering from the spin-polarized $k_x > 0$ states at the same position x.

of spin-up holes. Similarly to Ref. [36] in the time domain, with the weak hole-phonon scattering but relatively strong hole-hole Coulomb scattering at low temperature, the quasi-hot-hole Fermi distributions in the spatial domain are induced by the spin spatial precession frequency, which transfers spin-up holes near the corresponding Fermi energy into the spin-down states with the same energies, far higher than the Fermi energy of spin-down holes at large spin polarization. Consequently, as shown in Fig. 5, with the faster intervalley charge transfer rate of spin-down holes (from the K valley to the K' one), more holes are accumulated in the K' valley, leading to the valley polarization built up in the spatial domain.

1. Analytical analysis

We first focus on the analytical study of the induced valley polarization in the spatial domain by simplifying the KSBEs with only the hole-impurity and intervalley hole-phonon scatterings included. Then the spatial evolution of the valley polarization $P_v = (N_{K'} - N_K)/N_h$ is obtained as (refer to Appendix B)

$$\frac{\pi N_h}{m^2}\frac{\partial^2 P_v}{\partial x^2} = \frac{P_v}{\tau_p \tau_v^+} + \frac{P_s^{K'} - P_s^K}{2\tau_p \tau_v^-}. \tag{11}$$

Here, $1/\tau_v^{+(-)}$ represents the sum (difference) in the intervalley charge transfer rates between spin-up and spin-down holes. It can be seen that with the difference in the spin-diffusion lengths in the two valleys and the difference in the intervalley charge transfer rates between the spin-up and spin-down holes, the last term $(P_s^{K'} - P_s^{K'})/(\tau_p \tau_v^-)$ in Eq. (11) serves as the source term of the valley polarization, while the term $P_v/(\tau_p \tau_v^+)$ in Eq. (11) leads to the relaxation of the valley polarization.

From Eq. (11), the maximum valley polarization P_v^m along the diffusion direction can be approximately obtained as

$$P_v^m = \left.\frac{e^{-\beta_{\rm eff}^{\Downarrow}\omega_\xi} - e^{-\beta_{\rm eff}^{\Downarrow}\omega_\xi}}{e^{-\beta_{\rm eff}^{\Uparrow}\omega_\xi} + e^{-\beta_{\rm eff}^{\Uparrow}\omega_\xi}} \frac{P_s^{K'} - P_s^K}{2}\right|_{x=x_m}. \tag{12}$$

Here, $\beta_{\rm eff}^{\Downarrow(\Uparrow)} = 1/(k_B T_{\rm eff}^{\Downarrow(\Uparrow)})$ with k_B the Boltzmann constant; ω_ξ represents the intervalley phonon energy ($\omega_{K_6^L} = 17.5$ meV [36]). It can been seen from Eq. (12) that by increasing the difference in the spin polarizations between the two valleys, P_v^m can be enhanced. Moreover, with the larger difference in the Fermi energies between spin-up and spin-down holes through increasing the injected spin polarization or the hole density, the difference in the effective hot-hole temperatures between spin-up and spin-down holes becomes larger, leading to the increase of P_v^m.

The difference in the spin polarizations between the two valleys is plotted along the diffusion direction in the inset of Fig. 7(a) with all the relevant scatterings included. Together with the effective hot-hole temperatures from Fig. 6, an

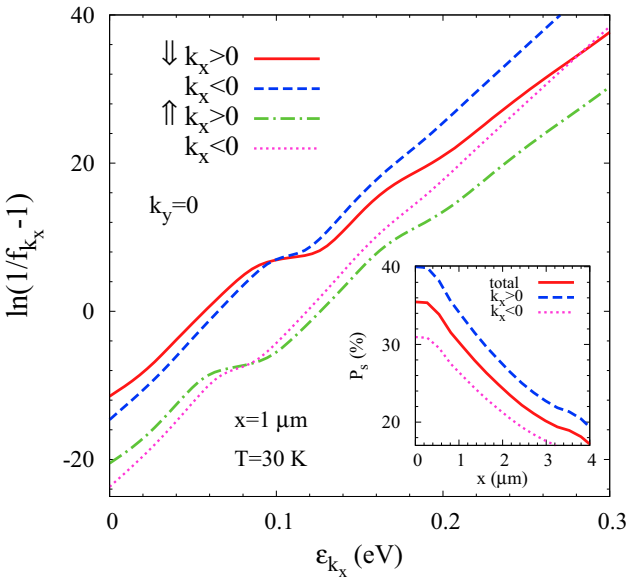

FIG. 6. Hole distribution versus ε_{k_x} for the states with $k_y = 0$ of spin-up and spin-down holes in the K valley at $x = 1$ μm. By fitting the slope of each curve, the corresponding effective hot-hole temperature is obtained: 72 K (68 K) for states with $k_x > 0$ of spin-up (spin-down) holes [solid (dot-dashed) curve]; 62 K (59 K) for states with $k_x < 0$ of spin-up (spin-down) holes [dashed (dotted) curve]. The inset shows the spin polarizations of $k_x > 0$ states (dashed curve), $k_x < 0$ states (dotted curve), and the entire system (solid curve). $N_h = 4 \times 10^{13}$ cm^{-2} and $P_s = 40\%$. $E_z = 0.03$ V/Å.

estimation of P_v^m can be obtained from Eq. (12). However, as seen from Fig. 6, it is noted that for both spin-up and spin-down holes, the effective hot-hole temperatures of $k_x > 0$ states are larger than those of $k_x < 0$ ones. Specifically, as shown in Fig. 5, at the left edge $x = 0$, the spin polarization $P^{\mu}_{s,k_x>0}(x = 0)$ of the $k_x > 0$ states in the distribution is fixed at P_s^0 in our calculation. In the region away from the boundary ($x > 0$), $P^{\mu}_{s,k_x>0}$ is induced due to the spin injection through the $k_x > 0$ states and $P^{\mu}_{s,k_x<0}$ is mainly induced through the scattering from the spin-polarized $k_x > 0$ states at the same position x. Consequently, in the steady state, with the relatively weak scattering at low temperature, $P^{\mu}_{s,k_x<0}$ is smaller than $P^{\mu}_{s,k_x>0}$, as shown in the inset of Fig. 6. Therefore, with the larger spin polarization and hence the larger difference in the Fermi energies between spin-up and spin-down holes of the $k_x > 0$ states in the distribution, the induced effective hot-hole temperature of the $k_x > 0$ states is larger than that of the $k_x < 0$ ones. The anisotropies of the effective hot-hole temperature and the spin polarization in the distribution make it complex to obtain an effective hot-hole temperature of the entire distribution in the spatial domain. Nevertheless, since the quasi-hot-hole Fermi distribution in the spatial domain is very similar to that in the time domain [36], except for the isotropy of the effective hot-hole temperature in the distribution in the time domain, we approximately take the effective hot-hole temperatures obtained from Ref. [36] in the similar condition, and then obtain an estimation of P_v^m from Eq. (12). Specifically, at $N_h = 4 \times 10^{13}$ cm^{-2} and $T = 30$ K, when $P_s^0 = 30\%$, with $|P_s^{K'} - P_s^K|_{\max} \approx 3.5\%$ [from the inset in Fig. 7(a)] and the effective hot-hole temperatures $T_{\rm eff}^{\Downarrow} = 74$ K and $T_{\rm eff}^{\Uparrow} = 66$ K (obtained from Ref. [36]), one has $P_v^m \approx 0.57\%$ from Eq. (12). Similarly, for the lager spin injection with $P_s^0 = 80\%$ at $N_h = 4 \times 10^{13}$ cm^{-2} and $T = 30$ K, the analytical estimation of P_v^m can exceed 1% ($|P_s^{K'} - P_s^{K'}|_{\max} > 5\%$ with the effective hot-hole temperatures [36] $T_{\rm eff}^{\Downarrow} = 150$ K and $T_{\rm eff}^{\Uparrow} = 112$ K).

2. *Numerical results*

We next discuss the valley polarization by numerically solving the KSBEs with all the relevant scatterings included. The valley polarizations P_v along the $\hat{\mathbf{x}}$ direction at different hole densities and injected spin polarizations are plotted in Fig. 7 when $T = 30$ K. To realize the large difference in the spin-diffusion lengths and hence the spin polarizations in the two valleys, the electric field in our calculation satisfies $\eta E_z = -\Omega_{\rm HF}(x = 0)$ for given hole density and injected spin polarization P_s^0. As seen from the figure, along the $\hat{\mathbf{x}}$ direction, the valley polarization first increases and then decays after reaching the maximum. This spatial dependence can be understood from Eq. (11). Near the boundary ($x = 0$), the source term $(P_s^{K'} - P_s^{K'})/(\tau_p \tau_v^-) \neq 0$ is more important than the relaxation one $P_v/(\tau_p \tau_v^+)$ in Eq. (11), since $P_v \approx 0$. Therefore, the valley polarization increases at the first several micrometers along the $\hat{\mathbf{x}}$ direction. In the region further away from the boundary ($x = 0$), due to the decay of the spin polarization, the HF EMF becomes weaker, leading to the smaller difference in the spin-diffusion lengths in the two valleys. Hence, the source term becomes weaker

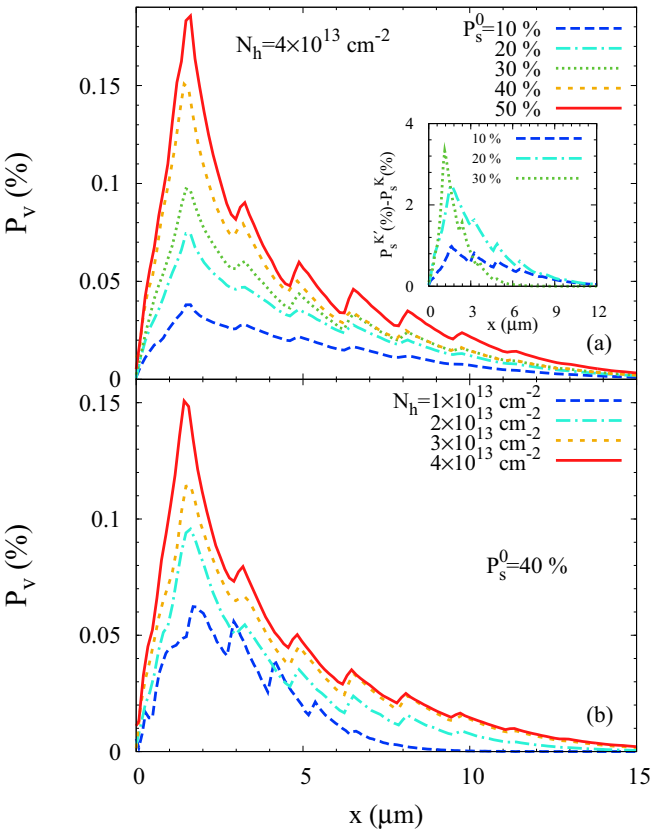

FIG. 7. The induced valley polarization P_v along the $\hat{\mathbf{x}}$ direction at different hole densities and injected spin polarizations when $T = 30$ K. The inset in (a) shows the difference in the spin polarizations between the two valleys along the diffusion direction.

whereas the relaxation term is stronger due to the buildup of the valley polarization. Consequently, the valley polarization starts to decay after reaching the maximum. Moreover, as shown in Fig. 7, the maximum valley polarization P_v^m along the $\hat{\mathbf{x}}$ direction increases with the spin polarization or hole density, qualitatively consistent with the analytical formula Eq. (12).

However, in contrast to the analytical estimation ($P_v^m \approx 0.57\%$ at $N_h = 4 \times 10^{13}$ cm^{-2} and $T = 30$ K for $P_s^0 = 30\%$), it is found that the valley polarization from the numerical calculation ($P_v^m \approx 0.1\%$) is much smaller in the same condition. This is due to the smaller spin polarization than the injected one near the injection boundary at low temperature. Specifically, as mentioned above, in the region away from the boundary ($x > 0$), $P^{\mu}_{s,k_x>0}$ is induced due to the spin injection through the $k_x > 0$ states and $P^{\mu}_{s,k_x<0}$ is induced through the scattering from the spin-polarized $k_x > 0$ states at the same position x. Consequently, with the relatively weak scattering at low temperature, one has $P^{\mu}_{s,k_x<0} < P^{\mu}_{s,k_x>0} \approx P_s^0$ near the injection boundary ($x \sim 0$), leading to the spin polarization P_s of the entire distribution smaller than the injected one P_s^0, as shown in the inset of Fig. 6. For the analytical study of the valley polarization in Sec. IV B 1, the effective hot-hole temperatures used in the estimation are obtained from Ref. [36] according to P_s^0. Therefore, with the smaller spin polarization P_s near the injection boundary in the numerical calculation, the

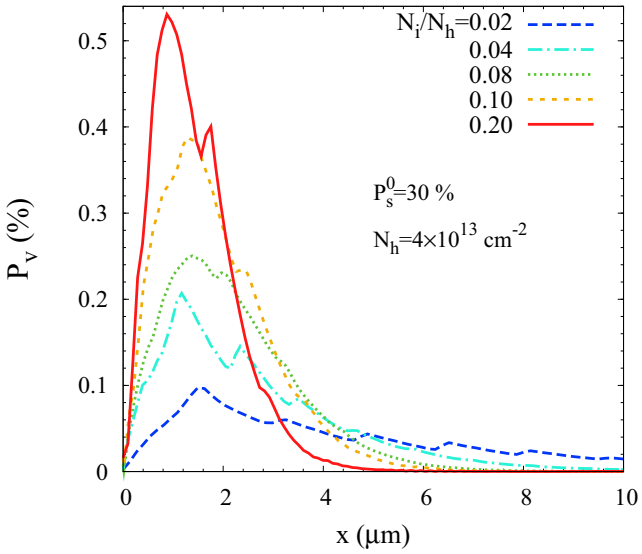

FIG. 8. The induced valley polarization P_v along the $\hat{\mathbf{x}}$ direction at different impurity densities when $N_h = 4 \times 10^{13}$ cm^{-2} and $P_s^0 = 40\%$. $T = 30$ K.

difference in the effective temperatures between the spin-up and spin-down holes is smaller, leading to smaller valley polarization.

By increasing impurity density to enhance the scattering strength, P_s near the injection boundary becomes closer to P_s^0, leading to the larger difference in the effective temperatures between the spin-up and spin-down holes and hence the enhanced P_v^m. Therefore, the maximum valley polarization along the $\hat{\mathbf{x}}$ direction increases with the impurity density, as shown in Fig. 8 where the valley polarizations along the $\hat{\mathbf{x}}$ direction are plotted at different impurity densities. This trend is very different from the time domain, in which the valley polarization always decreases with the increase of the intravalley scattering strength. Furthermore, it is noted that the increase of the scattering strength by increasing impurity density also enhances the decay of the valley polarization after reaching the maximum, which is due to the larger relaxation $[P_v/(\tau_p \tau_v^+)$ in Eq. (11)].

Moreover, as shown in Fig. 8, at large impurity density $N_i/N_h = 0.2$, P_v^m reaches 0.54% when $P_s^0 = 40\%$ with $T = 30$ K and $N_h = 4 \times 10^{13}$ cm^{-2}. This valley polarization from the full numerical calculation is very close to the simple estimation $P_v^m \approx 0.57\%$ in the same condition, and hence confirms the analytical formula Eq. (12). Furthermore, it is analytically revealed and numerically confirmed above that the larger valley polarization is expected with the increase of the injected spin polarization or hole density. Particularly, as mentioned above, from Eq. (12), the estimation of P_v^m can exceed 1% with the injected spin polarization reaching 80% when $N_h = 4 \times 10^{13}$ cm^{-2} and $T = 30$ K, providing the possibility for the experimental detection. Unfortunately, a full numerical computation at very large spin injection ($P_s^0 > 60\%$) or hole density ($N_h > 5 \times 10^{13}$ cm^{-2}) needs more grid points [54] in the momentum and real spaces and goes beyond our computing power.

V. SUMMARY

In summary, by the KSBE approach with all the relevant scatterings included, we have investigated the steady-state out-of-plane spin diffusion in p-type BL WSe_2 in the presence of the Rashba SOC and HF EMF. The out-of-plane component of the Rashba SOC serves as the opposite Zeeman-like fields in the two valleys. Together with the identical HF EMFs in the two valleys, the total EMF strengths are different in the two valleys. The intravalley spin-diffusion processes are shown to play an important role in the out-of-plane spin diffusion, and due to the valley-dependent total EMF strength, different intravalley processes in the two valleys can be obtained.

Specifically, it is shown that the intravalley spin-diffusion process in each valley can be divided into four regimes by tuning the total EMF strength in the corresponding valley. In different regimes, the spin-diffusion lengths show different dependencies on the scattering, total EMF, and SOC strengths. At small (large) injected spin polarization and hence the weak (strong) HF EMFs, the small (large) difference in the total EMF strengths in the two valleys is obtained, leading to the similar (different) spin-diffusion lengths in the two valleys. Moreover, we find that the intervalley hole-phonon scattering can suppress this difference in the spin-diffusion lengths at large spin injection but becomes marginal to the spin diffusion at small spin injection. It is further revealed that the suppression at large spin injection arises from the spin-conserving intervalley charge transfers with the opposite transfer directions between spin-up and spin-down holes by the intervalley hole-phonon scattering, which tends to suppress the difference in the spin polarizations in the two valleys. Therefore, with the increase of the intervalley hole-phonon scattering strength by increasing temperature, the difference in the spin-diffusion lengths in the two valleys at large spin injection becomes smaller.

Furthermore, with a fixed single-side large out-of-plane spin injection, it is found that a steady-state valley polarization along the spin-diffusion direction is built up at low temperature. Both analytical and numerical analyses show that it is induced due to the quasi-hot-hole Fermi distributions with different effective hot-hole temperatures between spin-up and spin-down holes induced during the spin diffusion, which leads to the different intervalley charge transfer rates in the opposite transfer directions, similarly to the induced valley polarization from the spin polarization in the time domain [36]. Nevertheless, different from the maximum valley polarization in the time domain, which always decreases with increasing the intravalley scattering, the one in the spatial domain is found to be enhanced by increasing the impurity density. This unique trend in the spatial domain is because the enhancement of the scattering leads to the total spin polarization near the injection boundary closer to the injected large value, which induces the larger difference in the effective hot-hole temperatures between spin-up and spin-down holes. The analytical results are confirmed by the full numerical calculation at large impurity density, and it is shown that larger valley polarization can be reached by increasing the hole density or injected spin polarization. Particularly, from the analytical estimation, the maximum valley polarization along the diffusion direction can exceed 1% at the experimental obtainable hole density and

with the injected spin polarization reaching 80%, providing the possibility for experimental detection.

ACKNOWLEDGMENTS

This work was supported by the National Natural Science Foundation of China under Grants No. 11334014 and No. 61411136001, the National Basic Research Program of China under Grant No. 2012CB922002, and the Strategic Priority Research Program of the Chinese Academy of Sciences under Grant No. XDB01000000.

APPENDIX A: ANALYTICAL ANALYSIS OF THE SPIN DIFFUSION

We analytically derive the out-of-plane spin-diffusion length in BL WSe_2 based on the KSBEs for the diffusion along the $\hat{\mathbf{x}}$ direction. In the steady state, with only the long-range hole-impurity scattering in the scattering terms, the KSBEs [Eq. (4)] are written as

$$k_x\partial_x\rho_{\mu\mathbf{k}}/m + i\nu E_z[k_x s_y - k_y s_x,\rho_{\mu\mathbf{k}}] + i\Omega_{\mathrm{T}}^{\mu}[s_z,\rho_{\mu\mathbf{k}}] + N_i\sum_{\mathbf{k}'}2\pi|V_{\mathbf{k}-\mathbf{k}'}|^2\delta(\varepsilon_{\mathbf{k}}-\varepsilon_{\mathbf{k}'})(\rho_{\mu\mathbf{k}}-\rho_{\mu\mathbf{k}'}) = 0. \quad \text{(A1)}$$

After the Fourier transformation

$$\rho_{\mu k}^{l} = \frac{1}{2\pi}\int_0^{2\pi} d\theta_{\mathbf{k}}\rho_{\mu\mathbf{k}}\exp(-il\theta_{\mathbf{k}}), \quad \text{(A2)}$$

Eq. (9) is obtained. In the strong ($l_\tau \ll l_\nu, l_{\Omega_{\mathrm{T}}^{\mu}}$) and moderate ($l_{\Omega_{\mathrm{T}}^{\mu}} \ll l_\tau \ll l_\nu$) scattering regimes, one only needs to keep the lowest two orders ($l = 0,1$) [59,62,63,67] and has

$$\begin{aligned} &l_\tau^2\{(r_{\Omega_{\mathrm{T}}^{\mu}}^2+1)\partial_x^2\rho_{\mu k}^0 - r_{\Omega_{\mathrm{T}}^{\mu}}^2[s_z,[s_z,\partial_x^2\rho_{\mu k}^0]] \\ &+2ir_{\Omega_{\mathrm{T}}^{\mu}}[s_z,\partial_x^2\rho_{\mu k}^0]\} + 2r_\nu l_\tau^2\{ir_{\Omega_{\mathrm{T}}^{\mu}}[s_x,\partial_x\rho_{\mu k}^0] \\ &+4ir_{\Omega_{\mathrm{T}}^{\mu}}[s_z,[is_y,\partial_x\rho_{\mu k}^0]] + (r_{\Omega_{\mathrm{T}}^{\mu}}^2+2)[is_y,\partial_x\rho_{\mu k}^0] \\ &-3r_{\Omega_{\mathrm{T}}^{\mu}}^2[s_z,[s_x,\partial_x\rho_{\mu k}^0]]\} + 2r_{\Omega_{\mathrm{T}}^{\mu}}^2(4r_\nu^2+3)[s_z,[s_z,\rho_{\mu k}^0]] \\ &-4r_\nu^2([s_x,[s_x,\rho_{\mu k}^0]] - [is_y,[is_y,\rho_{\mu k}^0]]) \\ &+2ir_{\Omega_{\mathrm{T}}^{\mu}}(2r_{\Omega_{\mathrm{T}}^{\mu}}^2 - 6r_\nu^2 - 1)[s_z,\rho_{\mu k}^0] = 0, \end{aligned} \quad \text{(A3)}$$

with $r_{\Omega_{\mathrm{T}}^{\mu}} = \Omega_{\mathrm{T}}^{\mu}\tau_{k,1}$ and $r_\nu = \nu k E_z\tau_{k,1}$.

By defining the spin vector $\mathbf{S}_\mu(x) = \mathrm{Tr}[\rho_{\mu k}^0(x)\boldsymbol{\sigma}]$, the equation of the out-of-plane spin vector in each valley can be given by

$$(\partial_x^6 + 3w\partial_x^4/l_\tau^2 + p\partial_x^2/l_\tau^4 - q/l_\tau^6)S_{\mu z} = 0, \quad \text{(A4)}$$

where $w = 4r_{\Omega_{\mathrm{T}}^{\mu}}^4(1+\bar{r}_\nu^2)/3$, $p = 16\bar{r}_\nu^4 + 4r_{\Omega_{\mathrm{T}}^{\mu}}^4(1+4\bar{r}_\nu^2 - 4\bar{r}_\nu^4 + r_{\Omega_{\mathrm{T}}^{\mu}}^2)$, and $q = 32r_\nu^2(4r_\nu^4 + r_{\Omega_{\mathrm{T}}^{\mu}}^2)$ with $\bar{r}_\nu^2 = r_\nu^2/|1+r_{\Omega_{\mathrm{T}}^{\mu}}^2|$. By solving this equation with the boundary condition $S_{\mu z}(0) = S_{\mu z}^0$ and $S_{\mu z}(+\infty) = 0$, the analytical solution of the spin polarization along the $\hat{\mathbf{x}}$ direction can be obtained as

$$S_{\mu z}(x) = A_o\exp(-x/l_s^o)\cos(x/L_o) + A_s\exp(-x/l_s^s), \quad \text{(A5)}$$

with $A_{o(s)}$ being the amplitude for the oscillatory (single-exponential) decay. The decay length $l_s^{o(s)}$ for the oscillatory (single-exponential) decay and the oscillation length L_o for the oscillatory decay are given by

$$l_s^s = l_\tau/\sqrt{\Gamma_{\mathrm{r}}}, \quad \text{(A6)}$$

$$l_s^o = \sqrt{2}l_\tau/\sqrt{\sqrt{|\Gamma_+|^2+|\Gamma_-|^2}+\Gamma_+}, \quad \text{(A7)}$$

$$L_o = 2l_\tau^2/|l_s^o\Gamma_-|, \quad \text{(A8)}$$

where

$$\Gamma_{\mathrm{r}} = -w + \sqrt[3]{b-\sqrt{b^2+d^3}} + \sqrt[3]{b+\sqrt{b^2+d^3}}, \quad \text{(A9)}$$

$$\Gamma_+ = -\frac{3}{2}w - \frac{\Gamma_{\mathrm{r}}}{2}, \quad \text{(A10)}$$

$$\Gamma_- = \frac{\sqrt{3}}{2}(\sqrt[3]{b-\sqrt{b^2+d^3}} - \sqrt[3]{b+\sqrt{b^2+d^3}}), \quad \text{(A11)}$$

with $b = q/2 + w(p-2w^2)/2$ and $d = p/3 - w^2$.

It is further found that the above analytical results can be reduced to simple forms in the four regimes defined in Sec. III A: I, the large total EMF and moderate scattering regime ($l_\tau \ll l_{\Omega_{\mathrm{T}}^{\mu}} \ll l_\nu$); II, the large total EMF and strong scattering regime ($l_{\Omega_{\mathrm{T}}^{\mu}} \ll l_\tau \ll l_\nu$); III, the crossover regime ($l_\tau \ll l_\nu \ll l_{\Omega_{\mathrm{T}}^{\mu}} \ll 2l_\nu^2/l_\tau$); and IV, the small total EMF regime ($l_\tau \ll l_\nu \ll 2l_\nu^2/l_\tau \ll l_{\Omega_{\mathrm{T}}^{\mu}}$). Specifically, for the single-exponential decay

$$l_s^s \approx \begin{cases} (l_\tau l_\nu)/(\sqrt{6}l_{\Omega_T^{\mu}}), & \text{regime I,} \\ l_\nu(1+l_\tau^2/l_{\Omega_T^{\mu}}^2)/\sqrt{2}, & \text{regime II,} \\ l_\nu(1-2l_{\Omega_T^{\mu}}^2 l_\tau^2/l_\nu^4)/\sqrt{2}, & \text{regime III,} \\ l_\nu/2, & \text{regime IV,} \end{cases} \quad \text{(A12)}$$

for the oscillatory decay

$$l_s^o \approx \begin{cases} \sqrt{2}l_\tau, & \text{regime I,} \\ l_{\Omega_T^{\mu}}, & \text{regime II,} \\ \sqrt{l_\tau l_{\Omega_T^{\mu}}}, & \text{regime III,} \\ l_\nu/(2\sqrt{2\sqrt{2}-1}), & \text{regime IV,} \end{cases} \quad \text{(A13)}$$

and the corresponding oscillation length

$$L_o \approx \begin{cases} l_{\Omega_T^{\mu}}/\sqrt{2}, & \text{regime I,} \\ l_\tau, & \text{regime II,} \\ \sqrt{l_\tau l_{\Omega_T^{\mu}}}, & \text{regime III,} \\ \sqrt{2\sqrt{2}+1}l_\nu/2, & \text{regime IV.} \end{cases} \quad \text{(A14)}$$

Additionally, one has $A_s \approx A_o$ only when $l_s^s \sim l_s^o$, and both the single-exponential decay and oscillatory decay are important with the nearly identical decay length. In other cases, the spin polarization exhibits either one single-exponential decay or oscillatory decay. In the large (small) total EMF regime [$l_{\Omega_T^{\mu}} \ll l_\nu$ ($2l_\nu^2/l_\tau \ll l_{\Omega_T^{\mu}}$)], the condition for the coexistence of single-exponential and oscillatory decays $l_s \approx l_o$ is never satisfied, and hence the steady-state spin polarization is approximated by one single-exponential (oscillatory) decay in this regime. In the crossover regime ($l_\nu \ll l_{\Omega_T^{\mu}} \ll 2l_\nu^2/l_\tau$), the condition for the coexistence of single-exponential and oscillatory decays $l_s^s \sim l_s^o$ can be satisfied, and hence there

exists strong competition between the single-exponential and oscillatory decays in this regime.

APPENDIX B: ANALYTICAL ANALYSIS OF THE VALLEY POLARIZATION

We next derive the spatial evolution of the valley polarization in the presence of the intervalley hole-phonon scattering. The KSBEs [Eq. (4)] with only the long-range hole-impurity and the intervalley hole-phonon scatterings are written as

$$\begin{aligned} &k_x\partial_x\rho_{\mu\mathbf{k}}/m + iv E_z[k_x s_y - k_y s_x,\rho_{\mu\mathbf{k}}] + i\Omega_{\mathrm{T}}^{\mu}[s_z,\rho_{\mu\mathbf{k}}] \\ &\quad + 2\pi N_i\sum_{\mathbf{k}'}|V_{\mathbf{k}\mathbf{k}'}|^2\delta(\varepsilon_{\mathbf{k}}-\varepsilon_{\mathbf{k}'})(\rho_{\mu\mathbf{k}}-\rho_{\mu\mathbf{k}'}) + \sum_{\mu'\mathbf{k}'}|M_\xi|^2 \\ &\quad \times\{[(\rho_{\mu\mathbf{k}}-\rho_{\mu\mathbf{k}'})n_\xi - \rho_{\mu'\mathbf{k}'}(1-\rho_{\mu\mathbf{k}})]\delta(\varepsilon_{\mathbf{k}'}-\varepsilon_{\mathbf{k}}-\omega_\xi) \\ &\quad + [(\rho_{\mu\mathbf{k}}-\rho_{\mu\mathbf{k}'})n_\xi + \rho_{\mu\mathbf{k}}(1-\rho_{\mu'\mathbf{k}'})]\delta(\varepsilon_{\mathbf{k}}-\varepsilon_{\mathbf{k}'}-\omega_\xi)\} \\ &\quad \times 2\pi\delta_{\mu',-\mu} = 0, \end{aligned} \tag{B1}$$

with n_ξ and $|M^\xi|$ being the phonon number and the momentum-independent scattering matrix element [36] of the intervalley phonon ξ mode ($\xi = K_6^L, K_6^H$), respectively.

It is noted that one has $n_\xi \approx 0$ at low temperature ($k_BT \ll \omega_\xi$). This indicates that the intervalley hole-phonon scattering through absorbing phonons can be neglected and the one through emitting phonons is important. After the Fourier transformation [Eq. (A2)], Eq. (B1) becomes

$$\begin{aligned} \frac{k}{2m}\frac{\partial^2}{\partial x^2}\left(\rho_{\mu\mathbf{k}}^{l-1}+\rho_{\mu k}^{l+1}\right) &= -i\Omega_{\mathrm{T}}^{\mu}\left[s_z,\rho_{\mu k}^{l}\right] - \frac{\rho_{\mu k}^{l}}{\tau_{k,l}} - I_{\mu k}^{l} \\ &\quad + \frac{kvE_z}{2}\left(\left[s_-,\rho_{\mu\mathbf{k}}^{l-1}\right] - \left[s_+,\rho_{\mu\mathbf{k}}^{l+1}\right]\right), \end{aligned} \tag{B2}$$

with

$$\begin{aligned} I_{\mu k}^{l} = m|M_\xi|^2\int\frac{d\epsilon_{k'}}{2\pi}\big[&\rho_{\mu k}^{l}\left(1-\rho_{-\mu k'}^{0}\right)\delta(\varepsilon_k-\varepsilon_{k'}-\omega_\xi) \\ &- \rho_{-\mu k'}^{0}\left(\delta_{l,0}-\rho_{\mu k}^{l}\right)\delta(\varepsilon_{k'}-\varepsilon_k-\omega_\xi)\big]. \end{aligned} \tag{B3}$$

Since the intervalley hole-phonon scattering is much weaker than the intravalley ones, one has $\rho_{\mu k}^{l}\tau_{k,l}^{-1} \gg I_{\mu k}^{l}$ in Eq. (B2) when $l \neq 0$ (it is noted that $\tau_{k,0}^{-1} = 0$). Therefore, as mentioned above, in the strong and moderate scattering regimes, one only needs to keep the lowest two orders ($l = 0,1$), and then obtains [62,63,67]

$$\begin{aligned} &l_\tau^2\left\{\left(r_{\Omega_{\mathrm{T}}^{\mu}}^2+1\right)\partial_x^2\rho_{\mu k}^{0} - r_{\Omega_{\mathrm{T}}^{\mu}}^2\left[s_z,\left[s_z,\partial_x^2\rho_{\mu k}^{0}\right]\right]\right. \\ &\quad \left. + 2ir_{\Omega_{\mathrm{T}}^{\mu}}\left[s_z,\partial_x^2\rho_{\mu k}^{0}\right]\right\} + 2r_v l_\tau^2\left\{ir_{\Omega_{\mathrm{T}}^{\mu}}\left[s_x,\partial_x\rho_{\mu k}^{0}\right]\right. \\ &\quad + 4ir_{\Omega_{\mathrm{T}}^{\mu}}\left[s_z,\left[is_y,\partial_x\rho_{\mu k}^{0}\right]\right] + \left(r_{\Omega_{\mathrm{T}}^{\mu}}^2+2\right)\left[is_y,\partial_x\rho_{\mu k}^{0}\right] \\ &\quad \left. - 3r_{\Omega_{\mathrm{T}}^{\mu}}^2\left[s_z,\left[s_x,\partial_x\rho_{\mu k}^{0}\right]\right]\right\} + 2r_{\Omega_{\mathrm{T}}^{\mu}}^2\left(4r_v^2+3\right)\left[s_z,\left[s_z,\rho_{\mu k}^{0}\right]\right] \\ &\quad - 4r_v^2\left(\left[s_x,\left[s_x,\rho_{\mu k}^{0}\right]\right] - \left[is_y,\left[is_y,\rho_{\mu k}^{0}\right]\right]\right) \\ &\quad + 2ir_{\Omega_{\mathrm{T}}^{\mu}}\left(2r_{\Omega_{\mathrm{T}}^{\mu}}^2 - 6r_v^2 - 1\right)\left[s_z,\rho_{\mu k}^{0}\right] - 6ir_{\Omega_{\mathrm{T}}^{\mu}}\left[s_z,\tau_{k,1}I_{\mu k}^{0}\right] \\ &\quad + 6r_{\Omega_{\mathrm{T}}^{\mu}}^2\left[s_z,\left[s_z,\tau_{k,1}I_{\mu k}^{0}\right]\right] - 2\left(r_{\Omega_{\mathrm{T}}^{\mu}}^2+1\right)\tau_{k,1}I_{\mu k}^{0} = 0. \end{aligned} \tag{B4}$$

The hole density in each valley $N_\mu = \mathrm{Tr}(\rho_{\mu\mathbf{k}}^{0})$. As the hole distribution exhibits a quasi-hot-hole Fermi distribution behavior during the spin diffusion (see Fig. 6), we use the hot-hole Fermi distribution $f_{\mu\mathbf{k}}^{\sigma} = 1/\{\exp[\beta_{\mathrm{eff}}^{\sigma}(\epsilon_{\mathbf{k}}-\mu_{\mu\sigma})]+1\}$ in the diagonal elements of the density matrices, and then obtain

$$\frac{\pi N_h^2}{2m^2}\frac{\partial^2}{\partial x^2}\left[P_{\mathrm{v}} + \frac{P_s^{K'2} - P_s^{K2}}{4}\right] = \frac{\Delta N^{\Uparrow}}{\tau_{k,1}\tau_{v\Uparrow}} - \frac{\Delta N^{\Downarrow}}{\tau_{k,1}\tau_{v\Downarrow}}. \tag{B5}$$

Here, $\Delta N^{\Uparrow(\Downarrow)} = N_{\mathrm{K}'(\mathrm{K})}^{\Uparrow(\Downarrow)} - N_{\mathrm{K}(\mathrm{K}')}^{\Uparrow(\Downarrow)}$ is the density difference for spin-up (spin-down) holes between the two valleys; $\tau_{v\Downarrow(\Uparrow)} = [e^{\beta(\omega_\xi - \Delta N^{\Downarrow(\Uparrow)}/D_s)} - 1]/(2m|M_\xi|^2)$ stands for the intervalley charge transfer time for spin-down (spin-up) holes with D_s being the density of states.

When all the relevant scatterings are included, $\tau_{k,1}$ in Eq. (B5) is replaced by τ_p. Moreover, with the suppression on the difference in the spin-diffusion lengths between the two valleys, we neglect the second term in the left of Eq. (B5), and then Eq. (11) is obtained with $1/\tau_v^{\pm} = 1/\tau_{v\Downarrow} \pm 1/\tau_{v\Uparrow}$. By assuming $\partial_x^2 P_{\mathrm{v}} = 0$ in Eq. (11) at $x = x_m$, where the valley polarization along the diffusion direction reaches the maximum, the maximum valley polarization [Eq. (12)] is obtained.

[1] K. S. Novoselov, D. Jiang, F. Schedin, T. J. Booth, V. V. Khotkevich, S. V. Morozov, and A. K. Geim, Proc. Natl. Acad. Sci. USA **102**, 10451 (2005).

[2] H. S. S. R. Matte, A. Gomathi, A. K. Manna, D. J. Late, R. Datta, S. K. Pati, and C. N. R. Rao, Angew. Chem. **122**, 4153 (2010).

[3] B. Radisavljevic, A. Radenovic, J. Brivio, V. Giacometti, and A. Kis, Nat. Nanotechnol. **6**, 147 (2011).

[4] S. B. Desai, G. Seol, J. S. Kang, H. Fang, C. Battaglia, R. Kapadia, J. W. Ager, J. Guo, and A. Javey, Nano Lett. **14**, 4592 (2014).

[5] H. Sahin, S. Tongay, S. Horzum, W. Fan, J. Zhou, J. Li, J. Wu, and F. M. Peeters, Phys. Rev. B **87**, 165409 (2013).

[6] X. D. Xu, W. Yao, D. Xiao, and T. F. Heinz, Nat. Phys. **10**, 343 (2014).

[7] B. Radisavljevic and A. Kis, Nat. Mater. **12**, 815 (2013).

[8] S. F. Wu, J. S. Ross, G. B. Liu, G. Aivazian, A. Jones, Z. Y. Fei, W. G. Zhu, D. Xiao, W. Yao, D. Cobden, and X. D. Xu, Nat. Phys. **9**, 149 (2013).

[9] H. T. Yuan, M. S. Bahramy, K. Morimoto, S. F. Wu, K. Nomura, B. J. Yang, H. Shimotani, R. Suzuki, M. Toh, C. Kloc, X. D. Xu, R. Arita, N. Nagaosa, and Y. Iwasa, Nat. Phys. **9**, 563 (2013).

[10] Z. R. Gong, G. B. Liu, H. Yu, D. Xiao, X. D. Cui, X. D. Xu, and W. Yao, Nat. Commun. **4**, 2053 (2013).

[11] D. Ovchinnikov, A. Allain, Y. S. Huang, D. Dumcenco, and A. Kis, ACS Nano **8**, 8174 (2014).

[12] A. M. Jones, H. Yu, J. S. Ross, P. Klement, N. J. Ghimire, J. Q. Yan, D. G. Mandrus, W. Yao, and X. D. Xu, Nat. Phys. **10**, 130 (2014).

[13] W. J. Zhu, T. Low, Y. H. Lee, H. Wang, D. B. Farmer, J. Kong, F. N. Xia, and P. Avouris, Nat. Commun. **5**, 3087 (2014).

[14] Y. F. Zhou, H. M. Xian, B. Wang, Y. J. Yu, Y. D. Wei, and J. Wang, J. Appl. Phys. **117**, 104307 (2015).
[15] D. H. Li, R. Cheng, H. L. Zhou, C. Wang, A. X. Yin, Y. Chen, N. O. Weiss, Y. Huang, and X. F. Duan, Nat. Commun. **6**, 7509 (2015).
[16] A. Splendiani, L. Sun, Y. Zhang, T. Li, J. Kim, C. Y. Chim, G. Galli, and F. Wang, Nano Lett. **10**, 1271 (2010).
[17] K. F. Mak, C. Lee, J. Hone, J. Shan, and T. F. Heinz, Phys. Rev. Lett. **105**, 136805 (2010).
[18] G. Eda, H. Yamaguchi, D. Voiry, T. Fujita, M. Chen, and M. Chhowalla, Nano Lett. **11**, 5111 (2011).
[19] Z. Y. Zhu, Y. C. Cheng, and U. Schwingenschlögl, Phys. Rev. B **84**, 153402 (2011).
[20] A. Ramasubramaniam, D. Naveh, and E. Towe, Phys. Rev. B **84**, 205325 (2011).
[21] D. Xiao, G. B. Liu, W. Feng, X. D. Xu, and W. Yao, Phys. Rev. Lett. **108**, 196802 (2012).
[22] K. Kaasbjerg, K. S. Thygesen, and K. W. Jacobsen, Phys. Rev. B **85**, 115317 (2012).
[23] T. Cheiwchanchamnangij and W. R. L. Lambrecht, Phys. Rev. B **85**, 205302 (2012).
[24] E. S. Kadantsev and P. Hawrylak, Solid State Commun. **152**, 909 (2012).
[25] K. Kośmider and J. Fernandez-Rossier, Phys. Rev. B **87**, 075451 (2013).
[26] F. Zahid, L. Liu, Y. Zhu, J. Wang, and H. Guo, AIP Adv. **3**, 052111 (2013).
[27] H. Shi, H. Pan, Y. W. Zhang, and B. I. Yakobson, Phys. Rev. B **87**, 155304 (2013).
[28] E. Cappelluti, R. Roldán, J. A. Silva-Guillén, P. Ordejón, and F. Guinea, Phys. Rev. B **88**, 075409 (2013).
[29] L. Debbichi, O. Eriksson, and S. Lebégue, Phys. Rev. B **89**, 205311 (2014).
[30] Y. Song and H. Dery, Phys. Rev. Lett. **111**, 026601 (2013).
[31] H. Ochoa and R. Roldan, Phys. Rev. B **87**, 245421 (2013).
[32] H. Ochoa, F. Guinea, and V. I. Fal'ko, Phys. Rev. B **88**, 195417 (2013).
[33] L. Wang and M. W. Wu, Phys. Lett. A **378**, 1336 (2014).
[34] L. Wang and M. W. Wu, Phys. Rev. B **89**, 115302 (2014).
[35] S. Dal Conte, F. Bottegoni, E. A. A. Pogna, D. De Fazio, S. Ambrogio, I. Bargigia, C. D'Andrea, A. Lombardo, M. Bruna, F. Ciccacci, A. C. Ferrari, G. Cerullo, and M. Finazzi, Phys. Rev. B **92**, 235425 (2015).
[36] F. Yang, L. Wang, and M. W. Wu, Phys. Rev. B **92**, 155414 (2015).
[37] L. Y. Yang, W. B. Chen, K. M. McCreary, B. T. Jonker, J. Lou, and S. A. Crooker, Nano Lett. **15**, 8250 (2015).
[38] T. Habe and M. Koshino, Phys. Rev. B **93**, 075415 (2016).
[39] L. Wang and M. W. Wu, Phys. Rev. B **89**, 205401 (2014).
[40] S. H. Liang, Y. Lu, B. S. Tao, S. M. Murtry, G. Wang, X. Marie, P. Renucci, H. Jaffres, F. Montaigne, D. Lacour, J. M. Georger, S. P. Watelot, M. Hehn, A. Djeffal, and S. Mangin, arXiv:1512.05022.
[41] Z. Yue, K. Tian, A. Tiwari, and M. E. Raikh, Phys. Rev. B **93**, 195301 (2016).
[42] M. W. Wu and C. Z. Ning, Eur. Phys. J. B **18**, 373 (2000); M. W. Wu, J. Phys. Soc. Jpn. **70**, 2195 (2001).
[43] M. W. Wu, J. H. Jiang, and M. Q. Weng, Phys. Rep. **493**, 61 (2010).
[44] M. I. D'yakonov and V. I. Perel', Zh. Eksp. Teor. Fiz. **60**, 1954 (1971) [Sov. Phys. JETP **33**, 1053 (1971)].
[45] Y. Yafet, Phys. Rev. **85**, 478 (1952).
[46] R. J. Elliott, Phys. Rev. **96**, 266 (1954).
[47] Y. A. Bychkov and E. I. Rashba, J. Phys. C **17**, 6039 (1984).
[48] A. Kormányos, V. Zólyomi, N. D. Drummond, and G. Burkard, Phys. Rev. X **4**, 011034 (2014).
[49] F. Meier and B. P. Zakharchenya, *Optical Orientation* (North-Holland, Amsterdam, 1984).
[50] D. D. Awschalom, D. Loss, and N. Samarth, editors, *Semiconductor Spintronics and Quantum Computation* (Springer, Berlin, 2002).
[51] T. Yu and M. W. Wu, Phys. Rev. B **89**, 045303 (2014).
[52] M. Q. Weng and M. W. Wu, Phys. Rev. B **68**, 075312 (2003).
[53] D. Stich, J. Zhou, T. Korn, R. Schulz, D. Schuh, W. Wegscheider, M. W. Wu, and C. Schüller, Phys. Rev. Lett. **98**, 176401 (2007); Phys. Rev. B **76**, 205301 (2007).
[54] J. L. Cheng and M. W. Wu, J. Appl. Phys. **101**, 073702 (2007).
[55] M. Q. Weng and M. W. Wu, Phys. Rev. B **66**, 235109 (2002); J. Appl. Phys. **93**, 410 (2003).
[56] J. L. Cheng, M. W. Wu, and I. C. da Cunha Lima, Phys. Rev. B **75**, 205328 (2007).
[57] T. Yu and M. W. Wu, Phys. Rev. A **92**, 013607 (2015).
[58] Y. Zhou and M. W. Wu, Phys. Rev. B **82**, 085304 (2010).
[59] B. Y. Sun and K. Shen, Solid State Commun. **151**, 1322 (2011).
[60] M. Ziese and M. J. Thornton (eds.), *Spin Electronics* (Springer, Berlin, 2001).
[61] Z. G. Yu and M. E. Flatté, Phys. Rev. B **66**, 201202 (2002).
[62] P. Zhang and M. W. Wu, Phys. Rev. B **79**, 075303 (2009).
[63] P. Zhang and M. W. Wu, Phys. Rev. B **84**, 045304 (2011).
[64] J. H. Jiang and M. W. Wu, Phys. Rev. B **79**, 125206 (2009).
[65] M. M. Glazov and E. L. Ivchenko, Zh. Eksp. Teor. Fiz. **126**, 1465 (2004) [J. Exp. Theor. Phys. **99**, 1279 (2004)].
[66] G. F. Giuliani and G. Vignale, *Quantum Theory of the Electron Liquid* (Cambridge University Press, Cambridge, 2005).
[67] P. Zhang, Y. Zhou, and M. W. Wu, J. Appl. Phys. **112**, 073709 (2012).